Stochastic Geometry Analysis of Radar-Communication Co-Existence in Vehicular Networks

Ankit Kumar*, Astitva Mehrotra†, and Gourab Ghatak*†, *Member IEEE*
*Bharti School of Telecommunications Technology & Management, IIT Delhi, India
†Department of Electrical Engineering, IIT Delhi, India
Emails: bsy227531@dbst.iitd.ac.in, eez238353@ee.iitd.ac.in, gghatak@ee.iitd.ac.in

***Abstract*—We employ tools of stochastic geometry to investigate the co-existence of millimeter wave (mm-wave) radar and communication features in vehicular networks with time and frequency resource sharing. First, we highlight the importance and applicability of signal to interference and noise ratio (SINR) as a metric to characterize the radar performance. Then, we define and characterize the probability of the joint event that the radar detection rate and the data communication rate exceed predetermined thresholds. We study the trends of the joint success probability either with time-division or frequency-division resource sharing between the radar and the communication functionalities. Furthermore, we define and optimize a metric called the effective range resolution (ERR) that jointly takes into account the detection probability with the bandwidth dedicated to the radar system. Our study highlights that although a frequency-division co-existence may improve radar detection probability due to reduced interference, it may eventually result in a higher ERR due to the reduced bandwidth. Accordingly, we provide key system design insights and prescribe different operation regimes for the co-existence system.**

I. Introduction

A. Context

As vehicles become increasingly connected and autonomous, the demand for both radar-based sensing for safety features and communication technologies for supporting vehicle-to-vehicle (V2V) and vehicle-to-infrastructure (V2I) applications is growing [1]–[3]. However, the shared electromagnetic spectrum between the radar and the data-transmission functionalities poses complexities in ensuring the seamless operation of these systems concurrently without interference. Two primary view points are popular in this aspect: (i) co-design of radar and communication waveforms and (ii) co-existence of radar and communication sub-systems. The co-design philosophy, with integrated radar and sensing waveforms offer a more efficient solution at the cost of increased complexity. Indeed, the fusion of radar and communication capabilities into a single cohesive unit better optimizes space, power, and cost efficiency. On the contrary, co-existence of the two sub-systems, albeit not an optimal design, achieves their concurrent operation via advanced access protocols for interference coordination. This results in a reduced signal processing complexity. We consider the second approach in this paper. The co-existence of radar and communication features in the millimeter wave (mm-wave) may either be in a time-shared or bandwidth-shared manner. In this paper, we investigate the impact of urban street geometry on the performance of time-shared and frequency-shared radar-communication co-existing subsystems. In particular, we consider a wireless network where base stationss (BSs) are deployed on the street intersections to maximize line of sight (LOS) coverage. To the best of our knowledge, a stochastic geometry analysis of the same has not been carried out in literature.

We acknowledge the support of the Bharti School of Telecommunications Technology & Management, IIT Delhi, for this work.

B. Related Work

Contrary to classical radar systems, in automotive radars, the EU project MOSARIM [4] experimentally discovered that the signals from interfering vehicles are unlikely to cause ghost targets like clutters. Rather, their impact is in creating noise-like combined interference. Most characterization of radar interference, however, are based on simulations and empirical approaches with complex ray-tracing and stochastic environments. This inhibits derivation of performance trends and system design insights. To alleviate this, stochastic geometry tools have gained popularity to facilitate the development of tractable models to analyze the performance of radar networks [5]–[8]. For the characterization of radar performance, such models not only consider randomly located clutter nodes in the environment [9] but also take into account the impact of interfering radars [10]. However, most stochastic geometry based approaches focus only on a single street system and hence ignores the traffic caused by intersections and oncoming vehicles from the neighboring streets. Additionally, for automotive systems, the aspect of joint radar and communication has limited studies. Indeed, the expanding use of mm-wave communication [11], [12] necessitates the implementation of meticulous spectrum and interference management strategies to ensure it coexists harmoniously with radar systems. Several recent studies have investigated the performance of radar systems in environments with coexisting radars. The authors in [5] propose a model where the distribution of vehicular radars is characterized as a Poisson Point Process (PPP). This statistical approach facilitates the derivation of the mean signal to interference plus noise ratio (SINR) experienced by a radar in such an environment. This mean SINR serves as a foundation for estimating key radar detection metrics, such as the probability of detection and the probability of false alarm. In [13], they propose the bistatic radar framework

ISBN 978-3-903176-65-2

across diverse scenarios like application in terrestrial settings while [14] extend it to space-based environments.

The authors in [15] perform a stochastic geometry analysis for joint radar communication system in mm-wave band. In particular, they demonstrate the impact of radar detection performance in the beam training of the communication subsystem. In [16], authors proposes a method for spectrum sharing between communication systems and automotive radars, mitigating interference between these systems. This enhances the reliability of automotive radars used for collision avoidance and improve the performance of communication systems operating in the same spectrum. The authors in [17] discuss integrating sensing and communication functionalities into a single system that could potentially lead to lower hardware costs and a more streamlined system design for vehicles, offering both object detection capabilities and data transmission capabilities, potentially enabling new applications in advanced driver-assistance systems (ADAS). The aforementioned approach delineated in [18] constitutes a structured mathematical framework intended for the comprehensive analysis and optimization of Joint sensing and communication (JSAC) systems. This framework systematically integrates fundamental elements such as BS, user equipment (UE), and sensing targets (ST), thereby providing a rigorous methodology for characterising the coverage probability and ergodic capacity of such systems.

The automotive radar network was expanded to a two-lane scenario in [19] by accommodating vehicles and smart traffic lights. Within this context, both vehicles and traffic lights are equipped with a dual-function radar and communication system, thereby embodying a multifaceted approach to vehicular communication and sensing. In [20], a methodology for multi-radar cooperative detection is introduced, aiming to enhance the detection region while establishing inter-radar communication links. Within this framework, radars are stratified into distinct tiers, with one radar designated as the fusion center in each tier. Other radars within the same tier are tasked with target detection and information collection, transmitting their findings to the fusion center. Power allocation strategies are also considered for both radar detection and communication tasks. Additionally, the cooperative detection region of the multi-radar system is rigorously analyzed, addressing the presence of overlapping detection regions among different radars. This analytical endeavor serves to ascertain the effectiveness and coverage of the cooperative detection mechanism, facilitating the optimization of detection performance across the collaborative radar network. Since the locations of the BS and the vehicles have become increasingly ad-hoc, across [18]–[20] it became apparent to the researchers that employing stochastic geometry is imperative to take into account the inherent randomness of the locations. However, despite the comprehensive modeling endeavors, no known study takes into account the impact of the street geometry, specifically the intersections and the BSs deployed on them on the radar detection and downlink communication performance.

C. Contributions and Organization

We consider a network consisting of vehicles as well as mm-wave BSs deployed along the streets of an urban environment. Based on this scenario, the salient contributions of this paper are as follows.

- First, we highlight the importance of the characterization of SINR from a radar detection perspective. Although this quantity has been studied in automotive radar networks recently, a justification of its efficacy in light of typical radar performance metrics such as detection probability and false alarm rate is missing from literature. Then, by employing the tools of stochastic geometry, we define and characterize the joint success probability of the SINR of the radar detection and the downlink SINR of the data communication to be respectively larger than two predetermined thresholds.
- In order to facilitate co-existence of the radar and the communication sub-systems in a vehicular network, we investigate asynchronous time-division multiple access (TDMA), bandwidth-sharing or frequency division multiple access (FDMA), both in mm-wave. The characterization for the TDMA operation is particularly challenging since the interfering nodes are common for the radar and the communication sub-systems. We derive accurate approximations for the joint success probability for the TDMA, while exact expressions are derived for the FDMA protocol. We highlight the advantages and drawbacks for each scheme and prescribe system design and operation rules to take advantage of each scheme.
- Based on the derived framework, we derive optimal resource partitioning of the time and frequency resources to maximize the joint success probability. We highlight that the FDMA system, due to reduced interference, the system has a higher joint success probability than the asynchronous TDMA system, albeit at the cost of a reduced bandwidth. In order to take the impact of the reduced bandwidth on the radar detection, we introduce a metric called the effective range resolution (ERR) that jointly takes into account the probability of detection and the range resolution of the radar, and study it for the different schemes.

II. System Model and Metrics of Interest

A. Network Geometry

Let us consider a 2D street system of a city modeled as a Poisson Line Process (PLP) $\Phi_{\rm L} \subset \mathbb{R}^2$ with intensity $\lambda_{\rm L}$. Each street in $\Phi_{\rm L}$ is uniquely characterized by the distance d between the origin O of the Euclidean plane and its projection P on the street and by the angle ψ between $\vec{OP}$ and the x-axis on the other hand. Thus, the set of parameters (ψ, d) forms a PPP of intensity $\lambda_{\rm L}$ on the half cylinder $\mathcal{D} := [0, 2\pi) \times \mathbb{R}^+$. On each street $L_i \in \Phi_{\rm L}$, we define the location of the vehicles as one-dimensional PPP $(\phi_{{\rm v}i})$, with intensity $\lambda_{\rm V}$. Accordingly, the locations of the vehicles form a Poisson Line Cox Process (PLCP). Let us consider the ego vehicle on the street L_1. The PPP of vehicles present in the street L_1 is denoted by $\Phi_{\rm v1}$. Furthermore, let us denote by $\Phi_{\rm vL}$, the point process generated by the intersections of $L_j \in \Phi_{\rm L}$ with line L_1, i.e., $\Phi_{\rm vL} = \{x_1 \in L_1 \cap L_j, L_1, \forall L_j \in \Phi_{\rm L}, j \neq 1\}$. In order to facilitate maximum LOS communication, let us assume that BSs are deployed on the street intersections. Such BSs effectively act as road-side units for vehicular users, while catering to pedestrian cellular users. Thus, the locations of the BSs are modeled according to $\Phi_{\rm vL}$. Here we assume that the strength of the received signals at the ego vehicle from the BSs located at intersections that are not in LOS are negligible. For high frequency mm-wave transmissions this is indeed practical [21], [22].

B. Propagation Model - Radar

Let transmit power of radars be P, and transmit and receive antenna gains be $G_{\rm t}$ and $G_{\rm r}$, respectively. We adopt the standard path-loss model with path-loss exponent α. Due to the wide variety of target vehicles, the target is assumed to have a fluctuating (random) RCS, $\sigma_{\rm c}$, which is an exponential random variable with mean $\bar{\sigma}$ based on the Swerling 1 model [23]. Thus, Probability Density Function (PDF) of the RCS $\sigma_{\rm c}$ is given by $f_{\sigma_{\rm c}}(\sigma) = (1/\bar{\sigma}) \exp(-\sigma/\bar{\sigma})$. Let the effective area of aperture be $A_{\rm e} = (G_{\rm r} c^2)/(4\pi f_{\rm c}^2)$ where c is speed of light and $f_{\rm c}$ is center frequency. Let the beamwidth of the radar be Ω, thus vehicles beyond this minimum distance $\delta = L/\tan(\Omega/2)$ can cause interference. Due to the strong line-of-sight link between the typical and the target vehicle, we assume that the desired signal does not suffer from any multipath and fading. This is consistent with recent literature on stochastic geometry-based studies of automotive radars, e.g., see [5]. Consequently, the reflected signal power from the target vehicle reaches the typical vehicle with signal-strength [24] is given by $S_{\rm R} = \gamma_1 \sigma_{\rm c} P R^{-2\alpha}$, where $\gamma_1 = (G_{\rm t} A_{\rm e})/(4\pi)^2$.

Let the coordinates of potential interfering vehicles be $\boldsymbol{z} = (x, L) \in \Phi_{\rm v1}$. Actually, the interference is caused due to transmitted radar signals from $\boldsymbol{z} \in \Phi_{\rm v1}^{'}$, where $\Phi_{\rm v1}^{'} = \{\boldsymbol{z} : \boldsymbol{z} \in \Phi_{\rm v1}, x \geq \delta\}$. Due to different scatterers in the environment, these signals experience multi-path fading, which is modeled as Rayleigh with variance 1, i.e., the fading power is exponentially distributed with mean 1. Note that our framework can be extended to any fading model by employing the corresponding fading distribution, in particular to Nakagami-m fading which is more appropriate for high-frequency transmissions. However, the choice of the fading model does not alter the insights and trends observed in this work. Hence, due to higher tractability, we assume Rayleigh fading model.

C. Propagation Model - Communication

Assume that BSs operates on mm-wave band. Since, mm-wave transmissions suffer heavily from blockages, communication becomes infeasible in case the link is blocked (in case of non-LOS). Accordingly, we assume that the power received from a BS whose signal is blocked by a building is null [22]. The path-gain at a distance d_r from a transmitter is given by $h_r K_r d_r^{-\alpha_r}$, where K_r and α_r are the path-loss coefficient and path-loss exponent, respectively. For each link we assume a Rayleigh fast fading h, with unit variance[1]. In our work, we assume a sectored model for the transmission pattern of the mm-wave antennas [26], consisting of a main-lobe of beamwidth θ, and a side-lobe. Let G_0 be the directivity gain product of the main-lobe transmitting and receiving antenna[2]. Let P_t be the transmit power of a BS, then, the received power from serving BS (nearest to ego vehicle) situated at a distance χ^* is given by $S_{\rm C} = G_0 P_t h_m K_m (\chi^*)_+{}^{-\alpha_m}$, where $(\chi*)_+ = \max\{1, \chi^*\}$ and $\chi^* = \arg\min_{\boldsymbol{\chi} \in \Phi_{\rm vL}} ||\boldsymbol{\chi}||$. The communication rate is calculated as

$$R_{\rm comm} = B_{\rm comm} \log_2(1 + \xi_{\rm C}), \tag{1}$$

where $B_{\rm comm}$ is the allocated bandwidth for communication and $\xi_{\rm C}$ is SINR experienced during the communication phase.

D. Communication Protocol

Due to the stationarity of $\Phi_{\rm v1}$, let us consider a typical vehicle at the origin. We focus only on the forward-looking radar of the vehicles and the downlink transmissions. The analysis for the backward-looking and side radars follows similarly. Moreover, the uplink and x-haul transmissions are assumed to be in a separate channel. The typical vehicle simultaneously performs two tasks - i) Radar detection, where it tracks a target vehicle and, ii) data reception, where it receives downlink status and critical sensing data from the nearest BSs. The radar-communication protocol based on resource sharing follows one of the strategies enumerated next.

1) **Option 1: Asynchronous TDMA.** Here the downlink reception and the radar detection functionalities at the vehicle are time-shared in the same mm-wave channel. However, since the sub-frame is optimized for each vehicle by the network, different vehicles may have distinct frame design. The transmit frames of length T are divided into two parts - i) radar detection for a duration $\beta_{\rm T} T$, and ii) downlink transmission for a duration $(1 - \beta_{\rm T})T$. During each function, the vehicle experiences interference from all the other BSs operating in the same band as well as from the radar transmissions of the other vehicles on the same street.
2) **Option 2: FDMA.** In this scheme the mm-wave band of bandwidth $B_{\rm m}$ is divided into the radar functionality ($\beta_{\rm B} B_{\rm m}$) and the communication functionality $(1 - \beta_{\rm B})B_{\rm m}$. In other words, the BS operate in a different channel as compared to the vehicular radars. Consequently, the radar signals experience interference

[1] Due to the low local scattering, a Nakagami fading is more suitable for mm-wave communications [25]. Such an assumption complicates the derived expressions without lending any extra insights to the system. However, our framework can be easily extended to more realistic fading models.

[2] For highly directional antennas, the side-lobe gain is negligible; thus, for simplicity, we assume it to be zero.

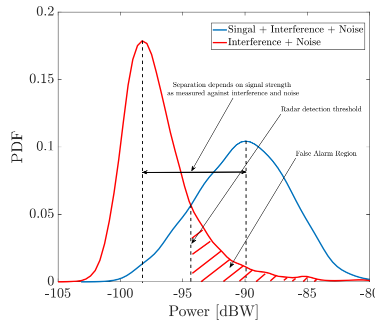

Fig. 1. Illustration of the importance of ξ_{R} in designing radar systems.

from the vehicles only, while the communication signals experience interference from the BSs only.

In the following section, we investigate each of the above schemes sequentially.

III. SINR, Radar Estimation Rate and Success Thresholds

A. Radar Estimation Rate

As discussed by author in [18], the concept of estimation rate emerges as a metric analogous to communication rate. This metric serves to quantify the information acquired regarding a target through the process of radar illumination. Estimation rate formally represents the minimal number of bits required to encode the Kalman residue, which signifies the statistical deviation from the predicted target parameter as determined by a Kalman filter. Thus, it represents the novel information content gleaned after subtracting the predicted target parameter, specifically since this predicted value is already established and does not contribute new information. Mathematically, it is denoted as

$$R_{\mathrm{est}} = B_{\mathrm{rad}} \log_2(1+\xi_{\mathrm{R}}). \tag{2}$$

where B_{rad} is the allocated bandwidth for detection of target vehicle and ξ_{R} is the SINR experienced during detection. Naturally, the probability that the radar estimation rate exceeds a threshold is equal to the probability that ξ_{R} is larger than a threshold η_{R}, to be defined later.

Let us illustrate the importance of characterizing ξ_{R} for designing radar systems with an example. Traditionally, radar networks are designed using the metrics of probability of detection and the probability of false alarm. The former is defined as the probability that the total received power including the useful signal and interference and noise exceeds a radar detection threshold. While, the latter is the probability that the interference and the noise exceeds the same threshold. In Fig. 1 we plot the corresponding distributions via Monte-Carlo simulations for a target distance of 10 m. The values of ξ_{R} determines how *well-separated* are the two distributions. Then, based on the distributions, and their relative separation, an appropriate radar detection threshold is selected that maximizes the detection probability subject to a predetermined false alarm probability. Thus, the larger the separation, the larger is the flexibility of selection of the radar detection threshold.

B. Interference and SINR Thresholds

Let χ be the distance of BS located at point $\boldsymbol{\chi}$ from the typical ego vehicle located at origin, i.e., $\chi = \|\boldsymbol{\chi}\|$. Let I_{R} and I_{C} be the interference at the typical vehicle at the radar detection and communication sub-systems respectively. Specifically,

$$I_{\mathrm{R}} = \begin{cases} \sum_{\boldsymbol{\chi}\in\Phi'_{\mathrm{vL}}} K_m G_0 P_{\mathrm{t}} h_m(\chi)_+^{-\alpha_m} + \\ \qquad\qquad \sum_{\boldsymbol{z}\in\Phi'_{\mathrm{v1}}} \gamma_2 P h_z \|\boldsymbol{z}\|^{-\alpha}; \text{ for TDMA} \\ \sum_{\boldsymbol{z}\in\Phi'_{\mathrm{v1}}} \gamma_2 P h_z \|\boldsymbol{z}\|^{-\alpha}; \text{ for FDMA} \end{cases} \tag{3}$$

$$I_{\mathrm{C}} = \begin{cases} \sum_{\boldsymbol{\chi}\in\Phi'_{\mathrm{vL}}} K_m G_0 P_{\mathrm{t}} h_m(\chi)_+^{-\alpha_m} + \\ \qquad\qquad \sum_{\boldsymbol{z}\in\Phi'_{\mathrm{v1}}} \gamma_2 P h_z \|\boldsymbol{z}\|^{-\alpha}; \text{ for TDMA} \\ \sum_{\boldsymbol{\chi}\in\Phi'_{\mathrm{vL}}} K_m G_0 P_{\mathrm{t}} h_m(\chi)_+^{-\alpha_m}; \text{ for FDMA} \end{cases} \tag{4}$$

where $\Phi'_{\mathrm{vL}} = \{\boldsymbol{\chi} : \boldsymbol{\chi} \in \Phi_{\mathrm{vL}}, ||\boldsymbol{\chi}|| \geq \chi^*\}$, $\gamma_2 = (G_{\mathrm{t}} A_{\mathrm{e}})/(4\pi)$, and h_z is the fading power. Accordingly,

$$\xi_{\mathrm{R}} = \frac{S_{\mathrm{R}}}{N_{\mathrm{R}} + I_{\mathrm{R}}},\ \xi_{\mathrm{C}} = \frac{S_{\mathrm{C}}}{N_{\mathrm{C}} + I_{\mathrm{C}}}$$

where

$$N_{\mathrm{R}} = \begin{cases} N_{\mathrm{d}} B_{\mathrm{m}} & ;\ \text{for TDMA} \\ N_{\mathrm{d}} \beta_{\mathrm{B}} Bm & ;\ \text{for FDMA} \end{cases} \tag{5}$$

$$N_{\mathrm{C}} = \begin{cases} N_{\mathrm{d}} B_{\mathrm{m}} & ;\ \text{for TDMA} \\ N_{\mathrm{d}} (1-\beta_{\mathrm{B}}) Bm & ;\ \text{for FDMA} \end{cases} \tag{6}$$

The threshold for detection calculated using (2) is given as,

$$\eta_{\mathrm{R}} = \begin{cases} 2^{\frac{\sigma_{\mathrm{est}}}{B_{\mathrm{m}}\beta_{\mathrm{T}} T}} - 1 & ;\ \text{for TDMA} \\ 2^{\frac{\sigma_{\mathrm{est}}}{\beta_{\mathrm{B}} B_{\mathrm{m}} T}} - 1 & ;\ \text{for FDMA} \end{cases} \tag{7}$$

and that for communication phase calculated using (1) is,

$$\eta_{\mathrm{C}} = \begin{cases} 2^{\frac{\sigma_{\mathrm{comm}}}{B_{\mathrm{m}}(1-\beta_{\mathrm{T}}) T}} - 1 & ;\ \text{for TDMA} \\ 2^{\frac{\sigma_{\mathrm{comm}}}{(1-\beta_{\mathrm{B}}) B_{\mathrm{m}} T}} - 1 & ;\ \text{for FDMA} \end{cases} \tag{8}$$

IV. Asynchronous TDMA Analysis

For asynchronous time-shared mm-wave transmission, the sub-frame time duration allotted for the radar detection and the communication phase is $\beta_{\mathrm{T}} T$ and $(1-\beta_{\mathrm{T}})T$ respectively. For both sub-systems, the entire bandwidth B_{m} is utilized. In this case, $I_{\mathrm{R}} = I_{\mathrm{C}}$ holds true from (3) and (4). Similarly, $N_{\mathrm{R}} = N_{\mathrm{C}}$ holds true from (5) and (6). Hence, joint probability of successful detection and communication $P_{\mathrm{s}}(\eta_{\mathrm{R}}, \eta_{\mathrm{C}})$ is:

$$\begin{aligned} &P_{\mathrm{s}}(\eta_{\mathrm{R}}, \eta_{\mathrm{C}}) \\ &\quad = \mathbb{P}(\xi_{\mathrm{R}} > \eta_{\mathrm{R}}, \xi_{\mathrm{C}} > \eta_{\mathrm{C}}) \\ &\quad = \mathbb{P}\left(\frac{\gamma_1 \sigma_{\mathrm{c}} P R^{-2\alpha}}{N_{\mathrm{R}} + I_{\mathrm{R}}} > \eta_{\mathrm{R}},\ \frac{G_0 P_t h_m K_m (\chi^*)^{-\alpha_m}}{N_{\mathrm{R}} + I_{\mathrm{R}}} > \eta_{\mathrm{C}} \right) \\ &\quad = \mathbb{P}(I_{\mathrm{R}} < \min(A, B)) \end{aligned}$$

where $A=\frac{\gamma_1\sigma_c PR^{-2\alpha}}{\eta_R}-N_R$, $B=\frac{G_0P_t h_m K_m(\chi^*)^{-\alpha_m}}{\eta_C}-N_R$. To evaluate further, we need the distribution of the random variable $E=\min\{A,B\}$. This is simply evaluated as

$$F_E(e)=\mathbb{P}(E\le e)=F_A(e)+F_B(e)-F_A(e)F_B(e) \quad (9)$$

where,

$$\begin{aligned}
F_A(e)&=\mathbb{P}\left(\frac{\gamma_1\sigma_c PR^{-2\alpha}}{\eta_R}-N_R\le e\right)\\
&=\mathbb{P}\left(\sigma_c\le\frac{\eta_R(e+N_R)}{\gamma_1PR^{-2\alpha}}\right)\overset{(a)}{=}1-\exp\left(-\frac{\eta_R(e+N_R)}{\bar{\sigma}\gamma_1PR^{-2\alpha}}\right)\\
F_B(e)&=\mathbb{P}\left(\frac{G_0P_th_mK_m(\chi^*)_+^{-\alpha_m}}{\eta_C}-N_C\le e\right)\\
&=\mathbb{P}\left(h_m\le\frac{\eta_C(e+N_C)}{G_0P_tK_m(\chi^*)_+^{-\alpha_m}}\right)\\
&\overset{(b)}{=}\mathbb{E}_a\left(1-\exp\left(-\frac{-\eta_C(e+N_C)}{G_0P_tK_m(\chi^*)_+^{-\alpha_m}}\right)\right)\\
&\overset{(c)}{=}1-4\lambda_L\\
&\int_0^\infty\exp\left(-\frac{\eta_C(e+N_C)}{G_0P_tK_m(\chi^*)_+^{-\alpha_m}}-4\lambda_L(\chi^*)_+\right)\mathrm{d}\chi^*
\end{aligned}$$

Step (a) follows from the exponential distribution of σ_c. In step (b), we are taking the average over fading. In step (c), we are taking the average over χ^*. Thus,

$$P_s(\eta_R,\eta_C)=\mathbb{P}(E>I_R)=\mathbb{E}(1-F_E(I_R)) \quad (10)$$

Now, recall that I_R for the TDMA case is the sum of the interference from the BSs as well as the radar nodes. Hence, solving (10) is challenging. Nevertheless, we provide a lower bound for the same assuming the independence of the events of successful radar detection as well as successful downlink transmission, i.e.,

$$P_s(\eta_R,\eta_C)\ge\mathbb{P}(\xi_R>\eta_R)\,\mathbb{P}(\xi_C>\eta_C). \quad (11)$$

In Section VI we will demonstrate that the bound is reasonably tight for the parameters under consideration.

Lemma 1. *The success probability $P_s(\eta_R)$ of radar detection is given by*

$$\mathbb{P}(\xi_R>\eta_R)=\int_0^\infty 4\lambda_L\mathcal{T}(R)\exp\left(-\lambda_V\mathcal{F}_{R1}-4\lambda_L\left(\mathcal{F}_{R2}+(\chi^*)_+\right)\right)\mathrm{d}\chi^* \quad (12)$$

where

$$\begin{aligned}
&||\mathbf{z}||=\sqrt{x^2+L^2},\mathcal{T}(R)=\exp\left(\frac{-\eta_RN_R}{\bar{\sigma}\gamma_1PR^{-2\alpha}}\right),\\
&\mathcal{F}_{R1}=\int_\delta^\infty 1-\frac{1}{1+\gamma'_{R1}||\boldsymbol{z}||^{-\alpha}}\,\mathrm{d}x,\ \gamma'_{R1}=\frac{4\pi\eta_R}{\bar{\sigma}R^{-2\alpha}},\\
&\mathcal{F}_{R2}=\int_{\chi^*}^\infty 1-\frac{1}{1+\gamma'_{R2}(\chi)_+^{-\alpha_m}}\,\mathrm{d}\chi,\ \gamma'_{R2}=\frac{\eta_RG_0K_mP_t}{\gamma_1\bar{\sigma}PR^{-2\alpha}}.
\end{aligned}$$

Proof. See Appendix A □

Lemma 2. *The probability $P_s(\eta_C)$ of successful downlink transmission is given by*

$$\mathbb{P}(\xi_C>\eta_C)=\int_0^\infty 4\lambda_L\mathcal{T}(C)\exp\left(-\lambda_V\mathcal{F}_{C1}-4\lambda_L\left(\mathcal{F}_{C2}+(\chi^*)_+\right)\right)\mathrm{d}\chi^* \quad (13)$$

where

$$\begin{aligned}
&\mathcal{T}(C)=\exp\left(\frac{-\eta_CN_R}{G_0P_tK_m(\chi^*)_+^{-\alpha_m}}\right),\\
&\mathcal{F}_{C1}=\int_\delta^\infty 1-\frac{1}{1+\gamma'_{C1}||\boldsymbol{z}||^{-\alpha}}\,\mathrm{d}x,\\
&\gamma'_{C1}=\frac{\eta_C\gamma_2P}{G_0P_tK_m(\chi^*)_+^{-\alpha_m}},\\
&\mathcal{F}_{C2}=\int_{\chi^*}^\infty 1-\frac{1}{1+\gamma'_{C2}(\chi)_+^{-\alpha_m}}\,\mathrm{d}\chi,\ \gamma'_{C2}=\frac{\eta_C}{(\chi^*)_+^{-\alpha_m}}
\end{aligned}$$

Proof. See Appendix B □

Thus, we have

$$P_s(\eta_R,\eta_C)\ge=\int_0^\infty 4\lambda_L(\mathcal{T}(R)\mathcal{T}(C)\exp(-\lambda_V(\mathcal{F}_{R1}+\mathcal{F}_{C1})-4\lambda_L(\mathcal{F}_{R2}+\mathcal{F}_{C2}+(\chi^*)_+)))\,\mathrm{d}\chi^* \quad (14)$$

We note that the success probabilities for both the radar detection and data transmission consists of three terms. The first accounts for the impact of noise, while the two other terms take into account the impact of radar interference and the BS interference, respectively. Next, we analyze the case when the radar transmissions and the downlink communication is scheduled in orthogonal frequency resources.

V. FDMA Analysis and ERR

For the frequency shared mm-wave transmission, the bandwidth allocated for radar detection is β_BB_m while for communication phase, the bandwidth is $(1-\beta_B)B_m$. For both sub-systems, entire time frame T is utilized.

Lemma 3. *The success probability $P_s(\eta_R)$ of radar detection for FDMA transmission is given by*

$$P_s(\eta_R)=\mathcal{T}(R)\exp\left(-\lambda_v\int_\delta^\infty 1-\frac{1}{1+\gamma'_{R1}||\boldsymbol{z}||^{-\alpha}}\,\mathrm{d}x\right) \quad (15)$$

Proof. See Appendix C. □

Lemma 4. *The success probability $P_s(\eta_C)$ for downlink communication in case of FDMA is given by*

$$P_s(\eta_C)=\int_0^\infty 4\lambda_L\mathcal{T}(C)\exp\left(-4\lambda_L\left(\mathcal{F}_{C2}+(\chi^*)_+\right)\right)\mathrm{d}\chi^* \quad (16)$$

Proof. See Appendix D. □

Unlike the asynchronous TDMA operation, in FDMA, since the two sub-systems operate in different frequencies, there is no inter-system interference. Hence, the SINR in both cases is independent of each other, leading to the exact result as discussed below.

Lemma 5. *The joint success probability is given by,*

$$\begin{aligned} P_{\rm s}(\eta_{\rm R}, \eta_{\rm C}) &= P_{\rm s}(\eta_{\rm R}) P_{\rm s}(\eta_{\rm C}) \\ &= \mathcal{T}(R) \exp\left(-\lambda_{\rm v} \int_{\delta}^{\infty} 1 - \frac{1}{1+\gamma'_{\rm R1}||\boldsymbol{z}||^{-\alpha}} \,{\rm d}x\right) \\ &\int_{0}^{\infty} 4\lambda_{\rm L} \mathcal{T}(C) \exp\left(-4\lambda_{\rm L}\left(\mathcal{F}_{\rm C2} + \chi^*\right)\right) {\rm d}\chi^* \end{aligned} \tag{17}$$

Although the interference is limited in case of the FDMA operation, the effective bandwidth allotted to the radar sub-system is lower. This has an impact on the range resolution of the radar, which is the ability of the radar system to distinguish between two targets that are close together in distance. The lower the bandwidth associated to the radar sub-system, the poorer will be the range resolution.

To take this into account, we define a metric ERR to judge the performance of radar and is given as,

$$\mathbf{ERR} = \Delta R P_{\rm s}(\eta_{\rm R}) + (1 - P_{\rm s}(\eta_{\rm R})) R \tag{18}$$

where $\Delta R = c/(2B_{\rm rad})$ is the range resolution of radar. Here, $B_{\rm rad} = B_{\rm m}$ and $B_{\rm rad} = \beta_{\rm B} B_{\rm m}$ for TDMA & FDMA respectively. This **ERR** determines how accurately we are able to locate the target.

Remark 1. *If ΔR for FDMA is more than the value of R at optimal $\beta_{\rm B}^*$ (which is meaningless), hence we would like to operate FDMA at $\beta_{\rm B}$ s.t. $c/(2RB_{\rm m}) \leq \beta_{\rm B} \leq 1$ (as $\Delta R \leq R$).*

VI. Numerical Results and Discussion

A. Optimal Time and Bandwidth Allocation Factor

Network parameters used are summarised in Table I. As shown in Fig. 2 (refer to (7) and (8)), there is a trade-off between $\eta_{\rm R}$ and $\eta_{\rm C}$ for different values of $\beta_{\rm T}$ and $\beta_{\rm B}$, and consequently, between success probabilities $P_{\rm s}(\eta_{\rm R})$ and $P_{\rm s}(\eta_{\rm C})$. Initially, $P_{\rm s}(\eta_{\rm R}, \eta_{\rm C})$ increases and then starts decreasing after attaining maximum value at $\beta_{\rm T}^* = 0.65$ and $\beta_{\rm B}^* = 0.09$ for TDMA and FDMA respectively.

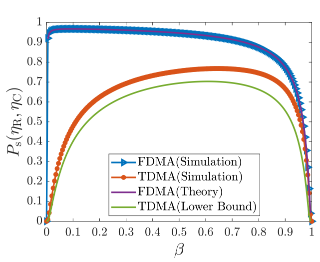

Fig. 2. $P_{\rm s}(\eta_{\rm R}, \eta_{\rm C})$ vs β for FDMA and TDMA

From Fig. 3a, we see that $\beta_{\rm B}^* = 0.09$ and $\beta_{\rm B}^* = 0.51$ for $\sigma_{est} = 10^2$ bits and $\sigma_{est} = 10^4$ bits respectively. From remark 1, we cannot use $\beta_{\rm B}^* = 0.09$ (as $\Delta R \geq R$), hence operate at

Network Parameter	Value
Transmit Power of Radar (P)	10 mW
Transmit Power of BS (P_t)	1 W
Lane Distance (L)	10 m
Mean RCS ($\bar{\sigma}$)	30 dbsm
Path Loss Exponent (α_m)	2
Path Loss Constant (K_m)	10^{-5}
Directivity Gain product (G_0)	10
Antenna Gain ($G_t = G_r$)	10 dBi
Center Frequency (f_C)	76.5 GHz
Noise Spectral Density ($N_{\rm d}$)	-174 dBm/Hz
Bandwidth ($B_{\rm m}$)	25 MHZ
Radar Beamwidth (Ω)	45°
$\sigma_{\rm est}$	10^2 bits
$\sigma_{\rm comm}$	10^4 bits
Length of Time Frame (T)	10 ms.

Table I: Network Parameters

$0.4 \leq \beta_{\rm B} \leq 1$. Since, $P_{\rm s}(\eta_{\rm R}, \eta_{\rm C})$ is a decreasing function of $\beta_{\rm B}$ when $0.4 \leq \beta_{\rm B} \leq 1$, we prefer to use $\beta_{\rm B} = 0.4$ as this value provides us the maximum $P_{\rm s}(\eta_{\rm R}, \eta_{\rm C})$ in the valid range. However, $\beta_{\rm B}^* = 0.51$ in latter case is valid value (as $\Delta R \leq R$).

As shown in Fig. 3b, we plot $P_{\rm s}(\eta_{\rm C})$ vs $P_{\rm s}(\eta_{\rm R})$ for FDMA and TDMA, which provides the operating region of both protocols. When the plot intersects the y-axis, it is the $\beta = 1$ point, and when plot intersects x-axis, it is the $\beta = 0$ point. We use $\beta_{\rm T} = 0.65$ and $\beta_{\rm B} = 0.4$ to find the partitions of time frame (of length T) for TDMA and mm-wave band (of bandwidth $B_{\rm m}$) for FDMA. For TDMA, time frame of length $T = 10$ ms. is divided into 6.5 ms. time for radar detection and 3.5 ms. time for downlink transmission. Similarly, for FDMA, we observe that mm-wave band of bandwidth $B_{\rm m}$ is divided into the bands of bandwidth 10 MHz and 15 MHz for radar functionality and communication functionality respectively.

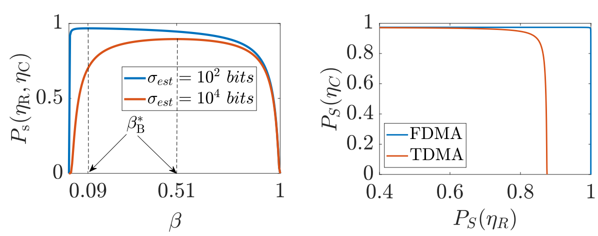

Fig. 3. (a) $P_{\rm s}(\eta_{\rm R}, \eta_{\rm C})$ vs β for different values of $\sigma_{\rm est}$ (FDMA), (b) Operating region for FDMA and TDMA

B. Variation of ERR and Success Probability with R

We plot **ERR** and $P_{\rm s}(\eta_{\rm R}, \eta_{\rm C})$ vs R for both FDMA & TDMA using $\beta_{\rm T} = 0.65$, $\beta_{\rm B} = 0.4$ and parameters mentioned in Table I. For different values of R, there can be two possibilities: Case I ($\Delta R \geq R \Rightarrow \beta_{\rm B} = \min\{1, c/(2RB_{\rm m})\}$) and Case II ($\Delta R \leq R \Rightarrow \beta_{\rm B} = 0.09$).

We first discuss FDMA protocol. Initially, for $0 \leq R \leq 6$, $\beta_{\rm B} = 1$ which means all bandwidth allotted for radar detection, hence, no communication occurs leading to outage. For

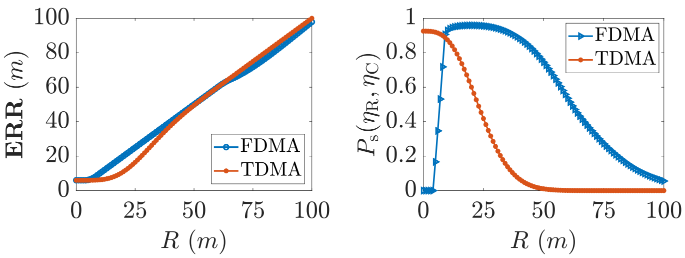

Fig. 4. (a) **ERR** for different values of R, (b) $P_{\mathrm{s}}(\eta_{\mathrm{R}}, \eta_{\mathrm{C}})$ for different values of R.

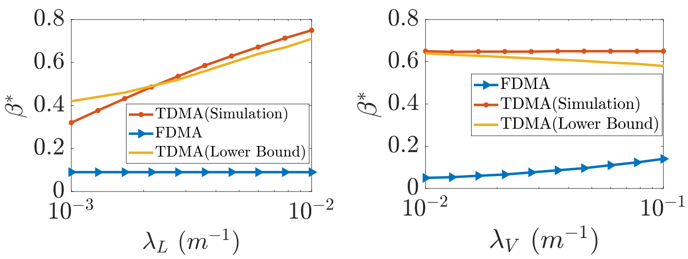

Fig. 5. (a) β^* vs λ_{L}, (b) β^* vs λ_{V}.

$6 \leq R \leq 20$, β_{B} rapidly decreases from 1 to 0.3 which leads to resource sharing between detection and communication, hence, increase in $P_{\mathrm{s}}(\eta_{\mathrm{R}}, \eta_{\mathrm{C}})$. Then, for $20 \leq R \leq 66.67$, β_{B} decreases slowly from 0.3 to 0.09 and R increases at much faster rate due to which S_{R} declines rapidly and $P_{\mathrm{s}}(\eta_{\mathrm{R}}, \eta_{\mathrm{C}})$ starts decreasing. When $R \geq 66.67$, β_{B} remains constant at 0.09 and $P_{\mathrm{s}}(\eta_{\mathrm{R}}, \eta_{\mathrm{C}})$ further decreases with increase in R.

For TDMA protocol, β_{T} is independent of R, hence, η_{R} and η_{C} remain constant. As R increases, S_{R} declines, leading to decrease in $P_{\mathrm{s}}(\eta_{\mathrm{R}}, \eta_{\mathrm{C}})$. For smaller values of R, first term in **ERR** is more dominant, hence, **ERR** remains constant. For large R, $P_{\mathrm{s}}(\eta_{\mathrm{R}})$ decreases as R increases due to which second term in **ERR** becomes more dominant and **ERR** increases.

C. Variation of β_{T}^* and β_{B}^* with λ_{L} and λ_{V}

Fig. 5 shows that as λ_{L} increases, S_{R} and I_{R} do not change for FDMA, hence, $P_{\mathrm{s}}(\eta_{\mathrm{R}})$ remains constant. Although, I_{C} increases, but, there is no change in $P_{\mathrm{s}}(\eta_{\mathrm{C}})$ as probability of connecting to nearer BS also increases leading to increase in S_{C}. So, β_{B}^* remains constant when λ_{L} increases from 10^{-3} to 10^{-2}. As λ_{V} increases, S_{R}, S_{C} and I_{C} remain constant but I_{R} increases for FDMA. So, more frequency resources needs to be assigned for radar functionality, hence, β_{B}^* increases. For TDMA protocol, $I_{\mathrm{C}} = I_{\mathrm{R}}$. As λ_{L} increases, interference I_{C} and I_{R} increase considerably as compared to when λ_{V} increases, since $P_t \geq P$. Hence, β_{T}^* shows a remarkable change when in the former case but shows negligible change in the latter. Currently, we are investigating performance of such co-existing radar systems in contrast to dedicated sub-system operations, e.g., mm-wave reserved for radar functionality and the data communication in the sub-6GHz band. This will be reported in a future work.

VII. Conclusion

We characterized the optimal partition of time frame and bandwidth between the radar and data communication sub-systems so as to maximize the joint success probability. FDMA mode of operation results in a lower interference experienced by both the sub-systems as compared to an asynchronous TDMA mode of operation. However, we cannot always rely on an optimal partition of bandwidth for FDMA since it may lead to unacceptable radar range resolution. Furthermore, we concluded that TDMA performs better than FDMA when the target vehicle is at small distance from the ego vehicle, whereas FDMA performs better for large distance target. A deeper investigation of the co-existence and comparing it with a dedicated sub-6GHz based data-communication system are being currently investigated.

Appendix A

The conditional success probability P_{s} is

$$P_{\mathrm{S}}(\eta_{\mathrm{R}}) = \mathbb{P}\left(\xi_{\mathrm{R}} > \eta_{\mathrm{R}}\right) = \mathbb{P}\left(\sigma_{\mathrm{c}} > \frac{\eta_{\mathrm{R}}(N_{\mathrm{R}} + I_{\mathrm{R}})}{\gamma_1 P R^{-2\alpha}}\right)$$

$$\stackrel{(a)}{=} \mathcal{T}(R)\mathbb{E}\left(\exp\left(\frac{-\eta_{\mathrm{R}}\sum_{\boldsymbol{z}\in\Phi'_{\mathrm{v}1}} \gamma_2 P h_z ||\boldsymbol{z}||^{-\alpha}}{\bar{\sigma}\gamma_1 P R^{-2\alpha}}\right)\right)$$

$$\mathbb{E}\left(\exp\left(\frac{-\eta_{\mathrm{R}}\sum_{\boldsymbol{\chi}\in\Phi'_{\mathrm{vL}}} G_0 K_m P_{\mathrm{t}} h_m(\chi)_+^{-\alpha_m}}{\bar{\sigma}\gamma_1 P R^{-2\alpha}}\right)\right)$$

$$= \mathcal{T}(R)\mathbb{E}\left(\prod_{\boldsymbol{z}\in\Phi'_{\mathrm{v}1}} \frac{1}{1 + \gamma'_{\mathrm{R}1}||\boldsymbol{z}||^{-\alpha}}\right)$$

$$\mathbb{E}\left(\prod_{\boldsymbol{\chi}\in\Phi'_{\mathrm{vL}}} \frac{1}{1 + \gamma'_{\mathrm{R}2}(\chi)_+^{-\alpha_m}}\right)$$

$$\stackrel{(b)}{=} \int_0^\infty 4\lambda_{\mathrm{L}}\mathcal{T}(R)\exp\left(-\lambda_{\mathrm{V}}\mathcal{F}_{\mathrm{R}1} - 4\lambda_{\mathrm{L}}\left(\mathcal{F}_{\mathrm{R}2} + \chi^*\right)\right) \mathrm{d}\chi^*$$

Step (a) follows from the exponential distribution of σ_{c} and step (b) follows from probability generating functional.

Appendix B

The conditional success probability P_{s} is

$$P_{\mathrm{s}}(\eta_{\mathrm{C}}) = \mathbb{P}\left(\xi_{\mathrm{C}} > \eta_{\mathrm{C}}\right) = \mathbb{P}\left(h_m > \frac{\eta_{\mathrm{C}}(N_{\mathrm{C}} + I_{\mathrm{C}})}{G_0 P_{\mathrm{t}} K_m (\chi^*)_+^{-\alpha_m}}\right)$$

$$\stackrel{(a)}{=} \mathcal{T}(C)\mathbb{E}\left(\exp\left(\frac{-\eta_{\mathrm{C}}\sum_{z\in\Phi'_{\mathrm{v}1}} \gamma_2 P h_z ||\boldsymbol{z}||^{-\alpha}}{G_0 P_{\mathrm{t}} K_m (\chi^*)_+^{-\alpha_m}}\right)\right)$$

$$\mathbb{E}\left(\exp\left(\frac{-\eta_{\mathrm{C}}\sum_{\boldsymbol{\chi}\in\Phi'_{\mathrm{vL}}} G_0 K_m P_{\mathrm{t}} h_m(\chi)_+^{-\alpha_m}}{G_0 P_{\mathrm{t}} K_m (\chi *)^{-\alpha_m}}\right)\right)$$

$$\stackrel{(b)}{=} \mathcal{T}(C)\mathbb{E}\left(\prod_{z\in\Phi'_{\mathrm{v}1}} \frac{1}{1 + \gamma'_{\mathrm{C}1}||\boldsymbol{z}||^{-\alpha}}\right)$$

$$\mathbb{E}\left(\prod_{\boldsymbol{\chi}\in\Phi'_{\mathrm{vL}}} \frac{1}{1 + \gamma'_{\mathrm{C}2}(\chi)_+^{-\alpha_m}}\right)$$

$$\overset{(c)}{=} \int_0^\infty 4\lambda_\mathrm{L}\mathcal{T}(C)\exp\left(-\lambda_\mathrm{V}\mathcal{F}_\mathrm{C1} - 4\lambda_\mathrm{L}\left(\mathcal{F}_\mathrm{C2} + (\chi^*)_+\right)\right)\mathrm{d}\chi^*$$

Step (a) follows from the exponential distribution of h_m, step (b) takes the average fading and step (c) follows from probability generating functional and then taking the average over χ^*.

Appendix C

The conditional success probability P_s is

$$\begin{aligned}
&P_\mathrm{S}(\eta_\mathrm{R}) = \mathbb{P}\left(\xi_\mathrm{R} > \eta_\mathrm{R}\right) = \mathbb{P}\left(\sigma_\mathrm{c} > \frac{\eta_\mathrm{R}(N_\mathrm{R}+I_\mathrm{R})}{\gamma_1 P R^{-2\alpha}}\right)\\
&\overset{(a)}{=} \mathcal{T}(R)\mathbb{E}\left(\exp\left(\frac{-\eta_\mathrm{R}\sum_{z\in\Phi'_\mathrm{v1}}\gamma_2 P h_z||\boldsymbol{z}||^{-\alpha}}{\bar{\sigma}\gamma_1 P R^{-2\alpha}}\right)\right)\\
&\overset{(b)}{=} \mathcal{T}(R)\mathbb{E}\left(\prod_{z\in\Phi'_\mathrm{v1}}\frac{1}{1+\gamma'_\mathrm{R1}||\boldsymbol{z}||^{-\alpha}}\right)\\
&\overset{(c)}{=} \mathcal{T}(R)\exp\left(-\lambda_\mathrm{v}\int_\delta^\infty 1 - \frac{1}{1+\gamma'_\mathrm{R1}||\boldsymbol{z}||^{-\alpha}}\,\mathrm{d}x\right)
\end{aligned}$$

Step (a) follows from the exponential distribution of σ_c, step (b) follows by taking average fading and step (c) follows from probability generating functional.

Appendix D

The conditional success probability P_s is

$$\begin{aligned}
&P_\mathrm{s}(\eta_\mathrm{C}) = \mathbb{P}\left(\xi_\mathrm{C} > \eta_\mathrm{C}\right) = \mathbb{P}\left(h_m > \frac{\eta_\mathrm{C}(N_\mathrm{C}+I_\mathrm{C})}{G_0 P_\mathrm{t} K_m (\chi^*)_+^{-\alpha_m}}\right)\\
&\overset{(a)}{=} \mathcal{T}(C)\mathbb{E}\left(\exp\left(\frac{-\eta_\mathrm{C}\sum_{\boldsymbol{\chi}\in\Phi'_\mathrm{vL}} G_0 K_m P_\mathrm{t} h_m (\chi)_+^{-\alpha_m}}{G_0 P_\mathrm{t} K_m (\chi^*)_+^{-\alpha_m}}\right)\right)\\
&= \mathcal{T}(C)\mathbb{E}\left(\prod_{\boldsymbol{\chi}\in\Phi'_\mathrm{vL}}\frac{1}{1+\gamma'_\mathrm{C2}(\chi)_+^{-\alpha_\mathrm{m}}}\right)\\
&\overset{(b)}{=} \int_0^\infty 4\lambda_\mathrm{L}\mathcal{T}(C)\exp\left(-4\lambda_\mathrm{L}\left(\mathcal{F}_\mathrm{C2} + (\chi^*)_+\right)\right)\mathrm{d}\chi^*
\end{aligned}$$

Step (a) follows from the exponential distribution of h_m and step (b) follows from probability generating functional and then taking the average over χ^*.

References

[1] H. Sarieddeen, N. Saeed, T. Y. Al-Naffouri, and M.-S. Alouini, "Next generation terahertz communications: A rendezvous of sensing, imaging, and localization," *IEEE Communications Magazine*, vol. 58, no. 5, pp. 69–75, 2020.

[2] X. You, C.-X. Wang, J. Huang, X. Gao, Z. Zhang, M. Wang, Y. Huang, C. Zhang, Y. Jiang, J. Wang *et al.*, "Towards 6g wireless communication networks: Vision, enabling technologies, and new paradigm shifts," *Science China Information Sciences*, vol. 64, pp. 1–74, 2021.

[3] Y. Chen, J. Zhang, W. Feng, and M.-S. Alouini, "Radio sensing using 5g signals: Concepts, state of the art, and challenges," *IEEE Internet of Things Journal*, vol. 9, no. 2, pp. 1037–1052, 2021.

[4] M. Kunert, "The EU project MOSARIM: A general overview of project objectives and conducted work," in *European Radar Conference*, 2012, pp. 1–5.

[5] A. Al-Hourani, R. J. Evans, S. Kandeepan, B. Moran, and H. Eltom, "Stochastic geometry methods for modeling automotive radar interference," *IEEE Transactions on Intelligent Transportation Systems*, vol. 19, no. 2, pp. 333–344, 2017.

[6] A. Munari, L. Simić, and M. Petrova, "Stochastic geometry interference analysis of radar network performance," *IEEE Communications Letters*, vol. 22, no. 11, pp. 2362–2365, 2018.

[7] J. Park and R. W. Heath, "Analysis of blockage sensing by radars in random cellular networks," *IEEE Signal Processing Letters*, vol. 25, no. 11, pp. 1620–1624, 2018.

[8] Z. Fang, Z. Wei, X. Chen, H. Wu, and Z. Feng, "Stochastic geometry for automotive radar interference with rcs characteristics," *IEEE Wireless Communications Letters*, 2020.

[9] A. R. Chiriyath and D. W. Bliss, "Effect of clutter on joint radar-communications system performance inner bounds," in *Asilomar Conference on Signals, Systems and Computers (ASILOMAR)*, 2015, pp. 1379–1383.

[10] G. M. Brooker, "Mutual interference of millimeter-wave radar systems," *IEEE Transactions on Electromagnetic Compatibility*, vol. 49, no. 1, pp. 170–181, 2007.

[11] N. Kouzayha, H. ElSawy, H. Dahrouj, K. Alshaikh, T. Y. Al-Naffouri, and M.-S. Alouini, "Analysis of large scale aerial terrestrial networks with mmwave backhauling," *IEEE Transactions on Wireless Communications*, vol. 20, no. 12, pp. 8362–8380, 2021.

[12] A. Faisal, H. Sarieddeen, H. Dahrouj, T. Y. Al-Naffouri, and M.-S. Alouini, "Ultramassive mimo systems at terahertz bands: Prospects and challenges," *IEEE Vehicular Technology Magazine*, vol. 15, no. 4, pp. 33–42, 2020.

[13] S. S. Ram and G. Ghatak, "Estimation of bistatic radar detection performance under discrete clutter conditions using stochastic geometry," in *2022 IEEE Radar Conference (RadarConf22)*. IEEE, 2022, pp. 1–6.

[14] S. Singhal, S. K. Biswas, and S. S. Ram, "Leo/meo-based multi-static passive radar detection performance analysis using stochastic geometry," in *2023 IEEE Radar Conference (RadarConf23)*. IEEE, 2023, pp. 1–6.

[15] Y. Nabil, H. ElSawy, S. Al-Dharrab, H. Attia, and H. Mostafa, "A stochastic geometry analysis for joint radar communication system in millimeter-wave band," in *ICC 2023-IEEE International Conference on Communications*. IEEE, 2023, pp. 5849–5854.

[16] C. Aydogdu, M. F. Keskin, N. Garcia, H. Wymeersch, and D. W. Bliss, "Radchat: Spectrum sharing for automotive radar interference mitigation," *IEEE Transactions on Intelligent Transportation Systems*, vol. 22, no. 1, pp. 416–429, 2019.

[17] D. Ma, N. Shlezinger, T. Huang, Y. Liu, and Y. C. Eldar, "Automotive dual-function radar communications systems: An overview," in *2020 IEEE 11th Sensor Array and Multichannel Signal Processing Workshop (SAM)*. IEEE, 2020, pp. 1–5.

[18] A. R. Chiriyath, B. Paul, and D. W. Bliss, "Radar-communications convergence: Coexistence, cooperation, and co-design," *IEEE Transactions on Cognitive Communications and Networking*, vol. 3, no. 1, pp. 1–12, 2017.

[19] F. De Saint Moulin, C. Wiame, L. Vandendorpe, and C. Oestges, "Joint performance metrics for integrated sensing and communication systems in automotive scenarios," *arXiv e-prints*, pp. arXiv–2208, 2022.

[20] Z. Fang, Z. Wei, Z. Feng, X. Chen, and Z. Guo, "Performance of joint radar and communication enabled cooperative detection," in *2019 IEEE/CIC International Conference on Communications in China (ICCC)*. IEEE, 2019, pp. 753–758.

[21] S. Salous and Y. Gao, "Wideband measurements in indoor and outdoor environments in the 30 ghz and 60 ghz bands," in *2016 10th European Conference on Antennas and Propagation (EuCAP)*. IEEE, 2016, pp. 1–3.

[22] White Paper, "5G Channel Model for bands up to 100 GHz," *http://www.5gworkshops.com/5gcm.html*, Dec. 6. 2015.

[23] D. Shnidman, "Expanded Swerling target models," *IEEE Transactions on Aerospace and Electronic Systems*, vol. 39, no. 3, pp. 1059–1069, 2003.

[24] D. P. Meyer and H. Meyer, "Review of the radar range equation," *Radar Target Detection-Handbook of Theory and Practice*, pp. 1–3, 1973.

[25] J. G. Andrews, T. Bai, M. N. Kulkarni, A. Alkhateeb, A. K. Gupta, and R. W. Heath, "Modeling and analyzing millimeter wave cellular systems," *IEEE Trans. Commun.*, vol. 65, no. 1, pp. 403–430, Jan. 2017.

[26] T. Bai and R. W. Heath, "Coverage and Rate Analysis for Millimeter-Wave Cellular Networks," *IEEE Trans. Wireless Commun.,*, vol. 14, no. 2, pp. 1100–1114, Feb. 2015.